arXiv:cond-mat/9709150v2 15 Sep 1997

Tuning the spin Hamiltonian of NENP by external pressure: a neutron scattering study

I. A. Zaliznyak[1,2†], D. C. Dender[1‡], C. Broholm[1,2], and Daniel H. Reich[1]
[1] *Department of Physics and Astronomy, The Johns Hopkins University, Baltimore, Maryland 21218*
[2] *National Institute of Standards and Technology, Gaithersburg, Maryland 20899*
(December 25, 2013)

Abstract

We report an inelastic neutron scattering study of antiferromagnetic spin dynamics in the Haldane chain compound $Ni(C_2H_8N_2)_2NO_2ClO_4$ (NENP) under external hydrostatic pressure $P = 2.5$ GPa. At ambient pressure, the magnetic excitations in NENP are dominated by a long-lived triplet mode with a gap which is split by orthorhombic crystalline anisotropy into a lower doublet centered at $\Delta_\perp \approx 1.2$meV and a singlet at $\Delta_\parallel \approx 2.5$meV. With pressure we observe appreciable shifts in these levels, which move to $\Delta_\perp(2.5\text{GPa}) \approx 1.45$ meV and $\Delta_\parallel(2.5\text{GPa}) \approx 2.2$meV. The dispersion of these modes in the crystalline $\hat{c}$-direction perpendicular to the chain was measured here for the first time, and can be accounted for by an interchain exchange $J'_c \approx 3\times10^{-4}J$ which changes only slightly with pressure. Since the average gap value $\Delta_H \approx 1.64$ meV remains almost unchanged with P, we conclude that in NENP the application of external pressure does not affect the intrachain coupling J appreciably, but does produce a significant decrease of the single-ion anisotropy constant from $D/J = 0.16(2)$ at ambient pressure to $D/J = 0.09(7)$ at $P = 2.5$ GPa.

PACS numbers: 75.10Jm, 75.40Gb, 75.50Ee.

Typeset using REVTEX

I. INTRODUCTION

The Haldane ground state [1] with short-range correlations and a gap to magnetic excitations has now been found in several quasi-one-dimensional S=1 antiferromagnets [2–6]. The magnetic properties of these materials are well-described by the spin Hamiltonian

$$\mathcal{H} = \sum_i \left\{ J\mathbf{S}_i \cdot \mathbf{S}_{i+1} + J' \sum_{\delta_\perp} \mathbf{S}_i \cdot \mathbf{S}_{i+\delta_\perp} + D(S_i^z)^2 \right\} \quad , \tag{1}$$

where in addition to the intrachain and interchain couplings J and J' we have included a uniaxial single-site anisotropy, a common feature of these systems. Because of its finite spin-spin correlation length, the Haldane state is stable with respect to small perturbations by the interchain exchange and single-ion anisotropy, and hence can be found not only in the pure 1D Heisenberg limit of Eq. (1), $J' = D = 0$, but for a finite range of J' and D around this point. If, however, the interchain coupling J' exceeds some critical value $J'_{crit.}$, quantum disorder is no longer favored and the system enters a long-range ordered Néel ground state with soft Goldstone excitations. Thus, a zero-temperature phase transition is expected to occur in a quasi-one-dimensional S=1 antiferromagnet at $J' = J'_{crit.}$ if the interchain coupling could be varied. Such quantum phase transitions have recently attracted much theoretical attention [7–14]. Various estimates using different model approximations [7–9] as well as numerical studies on finite systems [12] have been performed, giving values for the critical interchain coupling in the broad range $1.3 \times 10^{-3} \leq J'_{crit}/J \leq 2.6 \times 10^{-2}$. On the other hand, solid upper and lower limits on J'_{crit}/J are available from experiments. It is found that the hexagonal antiferromagnet $CsNiCl_3$ with $J \approx 2.8$ meV and $J'/J \approx 2 \times 10^{-2}$ undergoes 3D ordering at $T_N \approx 4.8$ K [15], while orthorhombic $Ni(C_2H_8N_2)_2NO_2ClO_4$ (NENP) with $J \approx 4$ meV and $J'/J \approx 8 \times 10^{-4}$ demonstrates all features of the Haldane system and remains disordered down to millikelvin temperatures [16].

The effects of single-ion anisotropy are less drastic than those of interchain coupling, but are also eventually critical. As the presence of the single-ion term in Eq. (1) does not change the basic 1D nature of the model, its effects may be readily explored by numerical simulations on finite systems of realistic size, and have been addressed in a number of studies [10–14]. These predict that strong Ising-like anisotropy ($D < 0$) favors Néel ordering for $D < -0.25J$, while "easy-plane" anisotropy ($D > 0$) eventually drives the system into a so-called "planar" phase at $D \approx J$ where all spins have $S^z = 0$ in the ground state.

The currently available experimental data on the effect of nonzero J' and D on the Haldane spin chain have been obtained from the comparison of results from different S=1 quasi-1D antiferromagnetic compounds. This restricts the experimentally accessible region of the (J', D) phase diagram discussed above to just a few points. However, the exchange and anisotropy parameters of the spin Hamiltonian can be controlled not only by changing the chemical composition of the magnetic compound, but also by tuning the properties of a single material. The application of hydrostatic pressure can change the interatomic separations and local atomic environments to which the spin Hamiltonian is highly sensitive, and therefore provides an opportunity for the controlled and continuous tuning of the parameters in the Hamiltonian, albeit in a restricted range. Here we report a study of the pressure dependence of the magnetic properties of NENP. We have used inelastic neutron scattering to measure the changes in the Haldane gap modes at $T \approx$1.8 K when an external pressure $P \approx 2.5$ GPa

is applied. We find that both the intrachain and interchain coupling are only marginally affected, but the single-ion anistropy is reduced substantially, and thus hydrostatic pressure drives this material closer to the ideal Heisenberg model and further away from any potential quantum phase transitions.

II. PROPERTIES OF NENP AT AMBIENT PRESSURE

NENP is orthorhombic with space group $Pnma$. It has Ni^{2+} chains stretching along the $\mathbf{b}$ direction with two chains per unit cell staggered in the $\mathbf{a}$ direction [17]. The ambient-pressure ($P \approx 0.1$ MPa) lattice parameters measured in our experiment at $T = 1.8$ K after the sample had been pressurized are $a = 15.28$ Å, $b = 10.23$ Å, and $c = 8.096$ Å. In describing neutron scattering experiments, we refer to wavevector transfer in the corresponding reciprocal lattice $\mathbf{Q} = h\mathbf{a}^* + k\mathbf{b}^* + l\mathbf{c}^* \equiv (h, k, l)$. Since the Ni^{2+} ions are displaced by $\mathbf{b}/2$ along the chain, it is convenient to refer to the component of wavevector transfer along the chain as $\tilde{q} = \mathbf{Q} \cdot (\mathbf{b}/2) = k\pi$ when discussing the 1D behavior of NENP. At ambient pressure the magnetic properties of NENP are well described by the Hamiltonian of Eq. (1) with $J = 4.0(2)$ meV, $D/J = 0.16(2)$, and an interchain coupling in the $\hat{a}$-direction $J'_a/J = 8 \times 10^{-4}$. The symmetry axis of the single-site anisotropy (z–axis) is parallel to the chain axis. The spin dynamics of NENP under these conditions have been carefully studied in a number of neutron-scattering experiments [2,3]. It was shown that the principal contribution to the spectral density of spin fluctuations $\mathcal{S}(\mathbf{Q}, \omega)$ comes from a triplet of long-lived excitations above a gap that follow a dispersion relation with fundamental periodicity in $\tilde{q}$ of 2π. Most of the spectral weight is concentrated in the close vicinity of the antiferromagnetic point $|\tilde{q} - \pi| < 2\pi/\xi \sim 0.3\pi$ (Here $\xi \sim$6–8 spins is the correlation length in the Haldane state). Over the full range $0.3\pi \leq \tilde{q} \leq \pi$ where they have been observed [3], these excitations are well-described by the single mode approximation (SMA):

$$\mathcal{S}^{\alpha\alpha}(\tilde{q}, \omega) = -\frac{2}{3}\left(\frac{\langle \mathcal{H} \rangle}{L}\right)\frac{1 - \cos\tilde{q}}{\hbar\omega_\alpha(\tilde{q})}\delta\left[\hbar\omega - \hbar\omega_\alpha(\tilde{q})\right] \quad , \tag{2}$$

where $\langle \mathcal{H} \rangle / L$ is the ground state energy per spin. The simplest dispersion relation that has the correct periodicity and adequately fits all the experimental data was found to be [3]

$$\hbar\omega_\alpha(\tilde{q}) = \sqrt{\Delta_\alpha^2 + v^2 \sin^2\tilde{q} + A\sin^2\frac{\tilde{q}}{2}} \tag{3}$$

with $v = 9.7$ meV, and $A = 34$ meV^2. Instead of a degenerate triplet excitation with a single gap $\Delta \approx 0.41J \approx 1.64$ meV at $\tilde{q} = \pi$ as expected in the isotropic case [13,14], the planar anisotropy in Eq. (1) splits the triplet into two branches with $\Delta_\parallel \approx 2.5$ meV and $\Delta_\perp \approx$1.2 meV for fluctuations polarized parallel and perpendicular to the chain axis, respectively. The lower mode is further split by a small orthorhombic anisotropy $\tilde{E}[(S_i^x)^2 - (S_i^y)^2]$ with $\tilde{E} \approx 0.01J = 0.04$ meV giving $\Delta_x \approx 1.34$ meV and $\Delta_y \approx 1.16$ meV [2]. This latter splitting is smaller than the instrumental resolution of our current experiment, and its effects will therefore be neglected in our subsequent discussion. The lower doublet also shows measurable dispersion along the $\mathbf{a}^*$ direction, with an effective bandwidth parameter $\Delta E \approx 0.65$ meV [2]. This is the basis of the above estimate of the interchain exchange J'_a. The dispersion along $\mathbf{c}^*$ has not been measured prior to this work.

III. EXPERIMENTAL PROCEDURE

Our sample was a 99% deuterated NENP single crystal of mass 0.27 g, which was a part of the composite sample used in Ref. [3]. The experiments were performed on the SPINS cold neutron triple-axis spectrometer at the National Institute of Standards and Technology. The beam divergences employed were $50'/k_i(\text{Å}^{-1}) - 80'$ around the vertically focussing pyrolytic graphite PG(002) monochromator, and $80' - 240'$ around the PG(002) analyzer. A liquid nitrogen cooled Be filter was placed in the scattered beam path. For constant-Q scans we fixed the final neutron energy E_f at 5.1 meV. The resulting full width at half maximum (FWHM) energy resolution for incoherent elastic scattering was $\Delta\hbar\omega = 0.27(1)$ meV. Scans with constant energy transfer $\hbar\omega = 2$ meV were performed with $E_f = 4.24$ meV to optimize the pressure cell transmission for both incident and scattered neutrons.

To provide high pressures, we used a clamp cell for neutron scattering supplied by Oval Co., Ltd., which is described in detail in Ref. [18]. The pressure was generated at room temperature by applying an external load of 2×10^5 N on the cap of the cylindrical sample chamber, or "microcell." The microcell is contained inside a barrel-shaped cylinder made of high-density polycrystalline Al_2O_3, which in turn is supported by steel rings. The microcell accommodated the parallelepiped-shaped NENP sample (dimensions $\approx 6\times6\times8$ mm^3), as well as a small NaCl platelet (dimensions $\approx 4 \times 4 \times 2$mm^3) used for pressure calibration. The microcell was filled with the pressure-transmitting fluid fluorinert FC-75 (available from 3M Chemicals, Inc.). The neutron beam reaches the sample through a 10 mm-high, continuous central window between the steel rings after passing through the Al_2O_3 pressure cylinder and the 5 mm-thick Al outer sleeve of the cell. The loaded cell was attached to the cold finger of a pumped He^4 cryostat for neutron scattering and cooled down to 1.8 K. Fig. 1 shows the transmission through the center of the loaded cell at $T = 1.8$ K for neutrons in the energy range $2 \le E \le 14$ meV (a reduced beam size $\approx 3 \times 3$ mm^2 was used for this measurement). The complicated structure of the curve indicates that the transmission is limited by Bragg diffraction from the Al_2O_3 cylinder. In the energy range $4 \le E \le 14$ meV, the measured cell transmission is well approximated by the superposition of three Gaussians,

$$T(E) = 0.085 + 0.031 \cdot \exp\left\{-\left(\tfrac{E-4.07}{0.283}\right)^2\right\} - 0.035 \cdot \exp\left\{-\left(\tfrac{E-5.3}{0.629}\right)^2\right\} + 0.021 \cdot \exp\left\{-\left(\tfrac{E-10.2}{3.58}\right)^2\right\} \quad , \tag{4}$$

as may be seen in Fig. 1. Scattering intensities measured at $P = 2.5$ GPa were subsequently corrected using the above expression for the energy-dependent transmission of the pressure cell normalized to unity for the constant-$\hbar\omega = 2$ meV scan. Specifically, the actual count rate was divided by

$$\tilde{T}(\hbar\omega) = \frac{\sqrt{T(E_f + \hbar\omega)T(E_f)}}{\sqrt{T(6.24\text{ meV})T(4.24\text{ meV})}} \approx 10\sqrt{T(E_f + \hbar\omega)T(E_f)}, \tag{5}$$

where E_f is the final neutron energy, and $T(E)$ is given by Eq. (4). The actual pressure applied to the sample at low temperatures in our experiment was $P \approx 2.5$ GPa, as determined from the measured change $\Delta a/a$=3.2×10^{-2} in the lattice constant of the NaCl sample [18].

For the reference measurements at ambient pressure we extracted the microcell with the sample from the pressure cell and placed it in a standard (ILL-type) flow cryostat. Its transmission for 5 meV neutrons measured the same way as above was 0.60(1), which can be attributed to incoherent scattering from the pressure-transmitting fluid and the NENP sample itself.

The sample was mounted with its (0,1,0) and (1,0,3) reciprocal lattice directions in the horizontal scattering plane. With this orientation, variations of the transverse (with respect to the spin chains) components of the wavevector transfer $\mathbf{Q} = (h, k, l)$ are coupled through $h = l/3$. However, the non-zero h had negligible effect in our experiment. First, recalling that inelastic neutron scattering only probes spin fluctuations polarized perpendicular to $\mathbf{Q}$ [19], we note that the (1,0,0) direction was $\approx 80^\circ$ out of the scattering plane. This means that at least 97% of the spin fluctuations polarized along $\mathbf{a}^*$ were always probed. Second, since the dispersion of the excitations along $\mathbf{a}^*$ has period 2 in h [2], it is quite negligible for $h < 0.2$ which is the case in present study. All constant-Q scans were performed at $k = 1$, i.e. with wavevector transfer along the chain $\tilde{q} = \pi$.

IV. RESULTS AND DISCUSSION

Our experimental results are shown in Figs. 2–5. The scattering intensity is shown normalized to 10 minutes counting time, although due to the low transmission of the pressure cell the bulk of the high-pressure data was counted three times this long to obtain adequate statistics. In Fig. 2 we present energy scans at $\mathbf{Q}$=(5/6,1,5/2). The large component of $\mathbf{Q}$ transverse to the chains means that more than 90% of the intensity of the longitudinally polarized (i.e. parallel to the chain axis) fluctuations is observed. At ambient pressure (0.1MPa) the corresponding gap is $\Delta_\parallel$= 2.49 meV, in agreement with previous studies [2,3]. At $P = 2.5$ GPa this mode shifts to lower energy, and is found at $\Delta_\parallel$(2.5 GPa) = 2.2 meV. The numbers quoted here are determined from the fits discussed below. In contrast, the energy of the transversely polarized mode, which at this $\mathbf{Q}$ primarily contains fluctuations polarized along $\mathbf{a}^*$, increases under pressure from $\Delta_\perp = 1.18$ meV to $\Delta_\perp$(2.5GPa) = 1.43 meV. This increase of the energy gap in the magnetic excitations spectrum qualitatively agrees with the results of recent heat capacity measurements [20] performed at pressures up to $\approx$ 0.5 GPa.

Figure 3 shows scans that probe the dispersion of the transversely polarized modes with wavevector transfer perpendicular to the chains $q_\perp \approx 2\pi l$. Presence of cell material in the beam cause much higher inelastic background and elastic scattering intensity in the high-pressure data. For $0 \leq l \leq 0.5$, $\mathbf{Q}$ makes angles between 0° and 33° with the chain direction, so that between 100% and 70% of the intensity of the $\mathbf{a}^*$-polarized transverse fluctuations and up to 30% of the intensity of the longitudinal fluctuations is measured. The latter is seen as a small rise after the main peak in the high-pressure data where the corresponding mode is centered at $\approx$ 2.2 meV. As shown in Fig. 4, a small shift of $\Delta_\perp$ to higher energies as l changes from 0.5 to 0 is clearly observed at ambient pressure. At P = 2.5 GPa, however, this shift is much smaller, and barely exceeds the experimental accuracy. Finally, one constant-$\hbar\omega = 2$ meV scan was performed at each pressure to probe the dispersion of the transverse fluctuations with $\tilde{q}$ along the chains. These scans are shown in Fig. 5.

The solid curves shown in Figs. 2–5 were obtained as a result of a global fit to all the data

at each pressure using the resolution-convoluted theoretical expression [19] for the neutron scattering cross-section based on the single-mode approximation (Eq. (2)) for $\mathcal{S}^{\alpha\alpha}(\mathbf{Q},\omega)$. To account for the dispersion perpendicular to the chains we used the dispersion relation

$$\hbar\omega_\alpha(\mathbf{Q}) = \sqrt{\Delta_\alpha^2 + v^2 \sin^2 \tilde{q} + A \sin^2 \frac{\tilde{q}}{2} + (\Delta E_\perp)^2 \frac{1-\cos\tilde{q}\cos q_\perp}{2}} \quad , \tag{6}$$

with $q_\perp = 2\pi l$. This was derived by adding in quadrature the energy of the Haldane modes given by Eq. (3) with the transverse dispersion obtained for magnons in spin-wave theory. We note that for $\tilde{q}$ close to π, Eq. (6) was obtained by Affleck [7] by treating the array of weakly interacting Haldane chains on the basis of the nonlinear sigma model. Except for the common parameters $\Delta_\parallel$, $\Delta_\perp$, v, $\Delta E_\perp$ in Eq. (6), for each scan only the individual constant background and gaussian intensity and width of the diffuse tail of incoherent scattering were varied in the global fit. Due to the limited range of $\tilde{q}$ probed, the parameter A was fixed at the value 34 meV^2 determined previously [3]. The results of the fits for the parameters in the dispersion relation are summarized in Table 1. The values χ^2=3.27 and χ^2(2.5GPa)=0.95 once more indicate the validity of the single mode approximation (2).

It can easily be shown within the framework of perturbation theory [21] that the single-ion anisotropy term $D\sum_i (S_i^z)^2$ gives a splitting of the initially isotropic Haldane triplet such that the average gap value remains unchanged: $\frac{1}{3}\Delta_\parallel + \frac{2}{3}\Delta_\perp = \Delta_H$. This fact can also be established with the symmetry arguments presented in the numerical study by Meshkov [13], where to $\sim 1\%$ accuracy the splitting was found to obey

$$\Delta_\parallel = \Delta_H + \frac{4}{3}D \quad , \qquad \Delta_\perp = \Delta_H - \frac{2}{3}D \quad , \tag{7}$$

so that $\Delta_\parallel - \Delta_\perp = 2D$. While we found that the average gap value Δ_H essentially did not change under pressure, the splitting of the gap decreased by more than 50%. This implies that only D is affected by hydrostatic pressure, while J remains unchanged. Using Eq. (7) we arrive at the value $D(2.5\text{ GPa}) = 0.09(7)J$ for the anisotropy constant as compared to $0.16(2)J$ under normal conditions. This result can be given a simple interpretation: since the hydrostatic pressure is isotropic, it tends to pack charge distributions inside the crystal more symmetrically, thereby reducing the local anisotropy. From the transverse dispersion parameter $\Delta E_\perp \sim 4S\sqrt{2J'J}$, we estimate the exchange along the $\mathbf{c}^*$ direction to be $J_c' \approx 3\times10^{-4}J$ and $J_c'(2.5\text{GPa}) \approx 2\times10^{-4}J$. This is even smaller than the value $J_a' \approx 8\times10^{-4}J$ in the $\mathbf{a}^*$ direction measured previously [2]. Thus J_c' appears to decrease with pressure, but this change is at the limit of our experimental accuracy.

V. CONCLUSIONS

In conclusion, changes in the spin dynamics of the Haldane gap antiferromagnet $Ni(C_2H_8N_2)_2NO_2ClO_4$ (NENP) under applied hydrostatic pressure of 2.5 GPa were studied by inelastic neutron scattering, and another point in the (D/J,J′/J) phase diagram of the S=1 spin system in the Haldane state has been attained experimentally. The principal effect of pressure was found to be a decrease by a factor 1.7 of the single-ion anisotropy constant in the spin Hamiltonian of the Ni^{2+} magnetic ions. This finding explains the increase with

pressure of the effective spin gap in NENP observed in the recent heat capacity measurements [20], as being the result of the increasing energy of the lower doublet component of the Haldane triplet. The exchange constant in the $\hat{c}$-direction perpendicular to the chains was also measured for the first time. It is smaller than the exchange along $\hat{a}$, and seems to decrease slightly with pressure. Thus the overall effect of applying hydrostatic pressure in NENP is not to move the system towards the phase transition to the Néel ordered ground state or the large-D planar phase but to bring it closer to the isotropic 1D limit.

VI. ACKNOWLEDGEMENTS

This work is based upon activities supported by National Science Foundation under agreement No. DMR-9413101. CB acknowledges support from the National Science Foundation through DMR-9453362. DHR acknowledges the support of the David and Lucile Packard Foundation.

REFERENCES

† Permanent affiliation: P. Kapitza Institute for Physical Problems, ul. Kosygina 2, 117334 Moscow, Russia.

‡ Present address: National Institute of Standards and Technology, Gaithersburg, MD 20899.

[1] F. D. M. Haldane, Phys. Lett. **93A**, 464 (1993); Phys. Rev. Lett. **50**, 1153 (1983).

[2] L.-P. Regnault, I. Zaliznyak, J. P. Renard and C. Vettier, Phys. Rev. B **50**, 9174 (1994), and references therein.

[3] S. Ma, D. Reich, C. Broholm, B. Sternlieb and R. W. Erwin, Phys. Rev. Lett. **69**, 3571 (1992); Phys. Rev. B **51**, 3289 (1995).

[4] G. Xu, J. F. DiTusa, T. Ito, K. Oka, H. Takagi, C. Broholm and G. Aeppli, Phys. Rev. B **54**, R6827 (1996), and references therein.

[5] H. Mutka, C. Payen, P. Molinie, J. L. Soubeyroux, P. Colombet and A. D. Taylor, Phys. Rev. Lett. **67**, 497 (1991); Physica B **180-181**, 197 (1992).

[6] V. Gadet, M Verdaguer, V. Briois, A. Gleizes, Phys. Rev. B 44, **44**, 705 (1991); L.-K. Chou, K.A. Abboud, D.R. Talham, W.W. Kim, and M.W.Meisel, Chem. Mater. **6**, 2051 (1994).

[7] I. Affleck, Phys. Rev. Lett. **62**, 474 (1989).

[8] M. Azzouz and B. Douçot, Phys. Rev. B **47**, 8660 (1993).

[9] D. Sénéchal, Phys. Rev. B **48**,15880 (1993).

[10] R. Botet, R. Jullien, and M. Kolb, Phys. Rev. B **28**, 3914 (1983).

[11] H. J. Schulz and T. Ziman, Phys. Rev. B **33**, 6545 (1986).

[12] T. Sakai and M. Takahashi, J. Phys. Soc. Jpn. **58**, 3131 (1989); Phys. Rev. B **42**, 4537 (1990).

[13] S. V. Meshkov, Phys. Rev. B **48**, 6167 (1993).

[14] O. Golinelli, Th. Jolicoeur and R. Lacaze, J. Phys.: Condens. Matter **5**, 7847 (1993); Phys. Rev. B **46**, 10854 (1992).

[15] W. B. Yelon and D. E. Cox, Phys. Rev. B **6**, 204, (1972); **7**, 2024 (1973).

[16] O. Avenel *et al.*, J. Low Temp. Phys. **89**, 547 (1992).

[17] A. Meyer *et al.*, Inorg. Chem. **21**, 1729 (1982).

[18] A. Onodera, Y. Nakai, N. Kunitomi, O. A. Pringle, H. G. Smith, R. M. Nicklow, R. M. Moon, F. Amita, N. Yamamoto, S. Kawano, N. Achiwa and Y. Endoh, Japanese Journ. Appl. Phys. **26**, 152 (1987).

[19] S. W. Lovesey, *Theory of Neutron Scattering from Condensed Matter* (Clarendon, Oxford, 1984).

[20] M. Ito, H. Yamashita, T. Kawae and K. Takeda, J. Phys. Soc. Jpn. **66**, 1265, (1997).

[21] L.-P. Regnault, I. A. Zaliznyak and S. V. Meshkov, J. Phys.: Condens. Matter, **5** L677, (1993).

FIGURES

FIG. 1. Energy dependence of neutron transmission for the pressure cell loaded with our NENP sample at $T = 1.8$ K. The solid line is an approximate fit given in Eq. (4).

FIG. 2. Constant-$\mathbf{Q}$ scans at $\mathbf{Q} = (.833, 1, 2.5)$ picking up both transverse and longitudinal fluctuations at $P = 2.5$ GPa (top) and $P = 0.1$ MPa (bottom).

FIG. 3. Scans at different $\tilde{q}_\perp$ probing the dispersion of the transverse fluctuations with wavevector transfer perpendicular to the chains: (a)–(c) $P = 2.5$ GPa; (d) and (e) $P = 0.1$ MPa.

FIG. 4. Dispersion curves for the transverse polarized gap mode obtained with Eq. (6) using parameters from Table 1. Open symbols and error bars were obtained from independent unconstrained fits of each individual peak with the resolution convoluted lineshape.

FIG. 5. Constant-$\hbar\omega$ scans sensitive to the velocity of excitations along the chains at $P = 2.5$ GPa (top) and $P = 0.1$ MPa (bottom).

TABLES

TABLE I. Summary of the dispersion parameters obtained from the global fits to data at two pressures; Δ_H is the average gap defined with Eq. (7).

Pressure (Pa)	$\Delta_\perp$ (meV)	$\Delta_\parallel$ (meV)	Δ_H (meV)	v (meV)	$\Delta E_\perp$ (meV)
10^5	1.180(4)	2.49(1)	1.62(1)	9.34(20)	0.43(3)
$2.5{\cdot}10^9$	1.426(6)	2.20(2)	1.68(2)	9.47(20)	0.32(7)

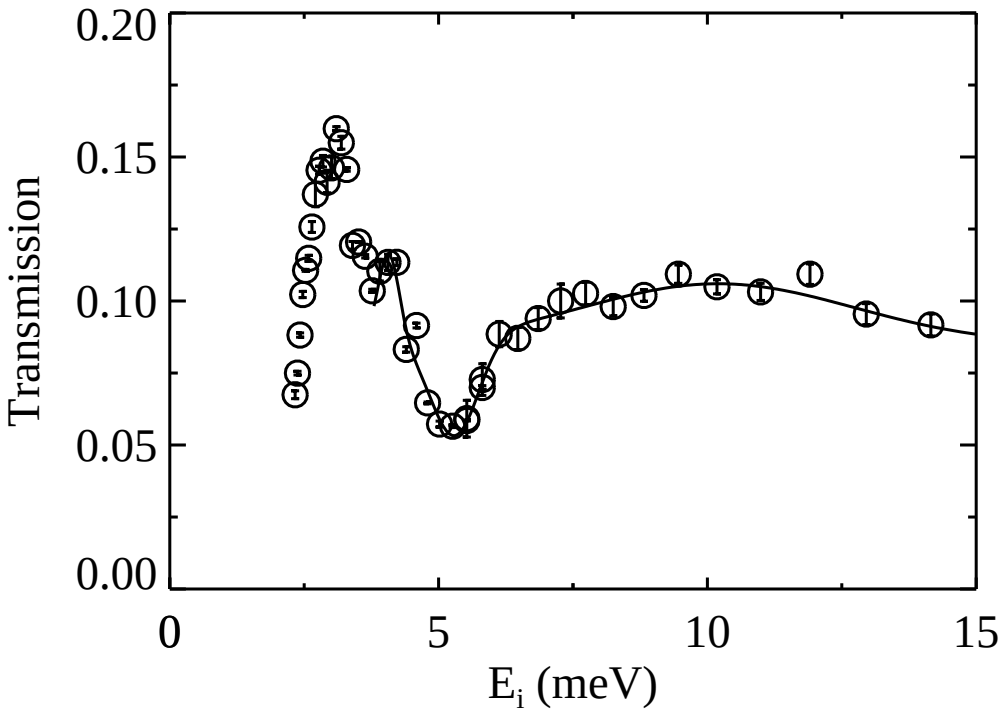

Figure 1

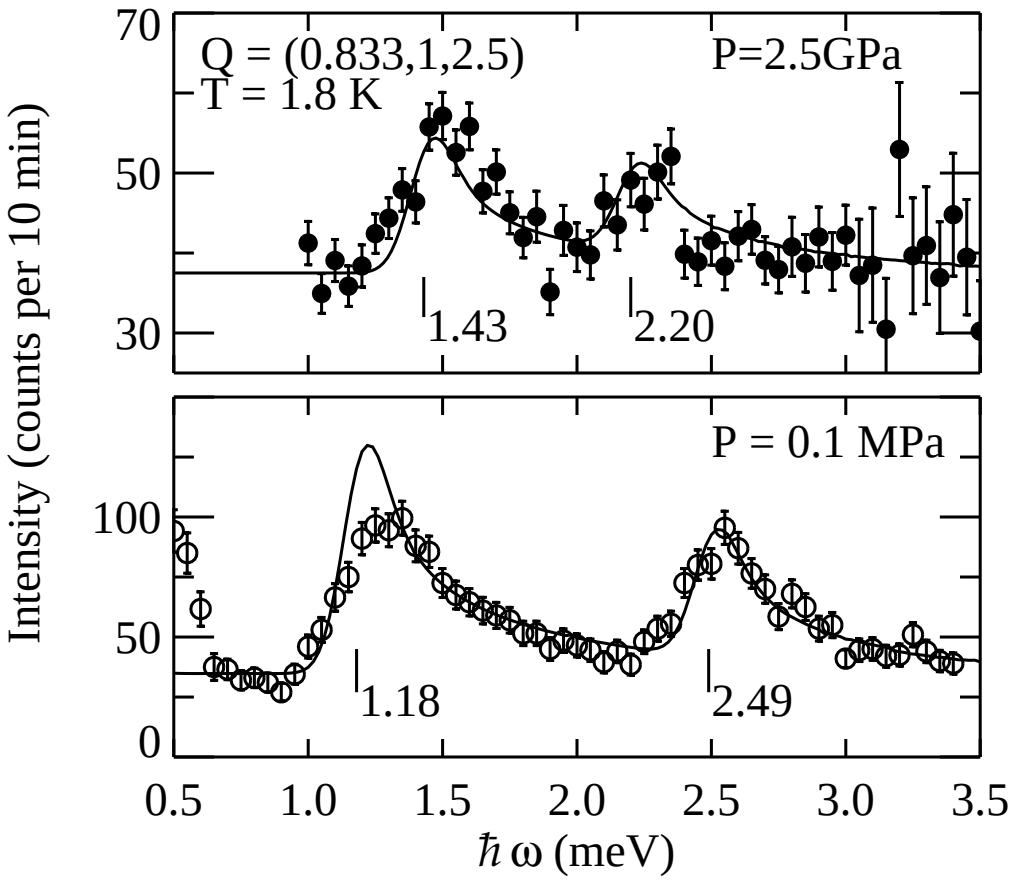
Q = (0.833,1,2.5)
T = 1.8 K
P=2.5GPa
1.43
2.20
P = 0.1 MPa
1.18
2.49
Intensity (counts per 10 min)
ħ ω (meV)
70
50
30
100
50
0
0.5
1.0
1.5
2.0
2.5
3.0
3.5

Figure 2

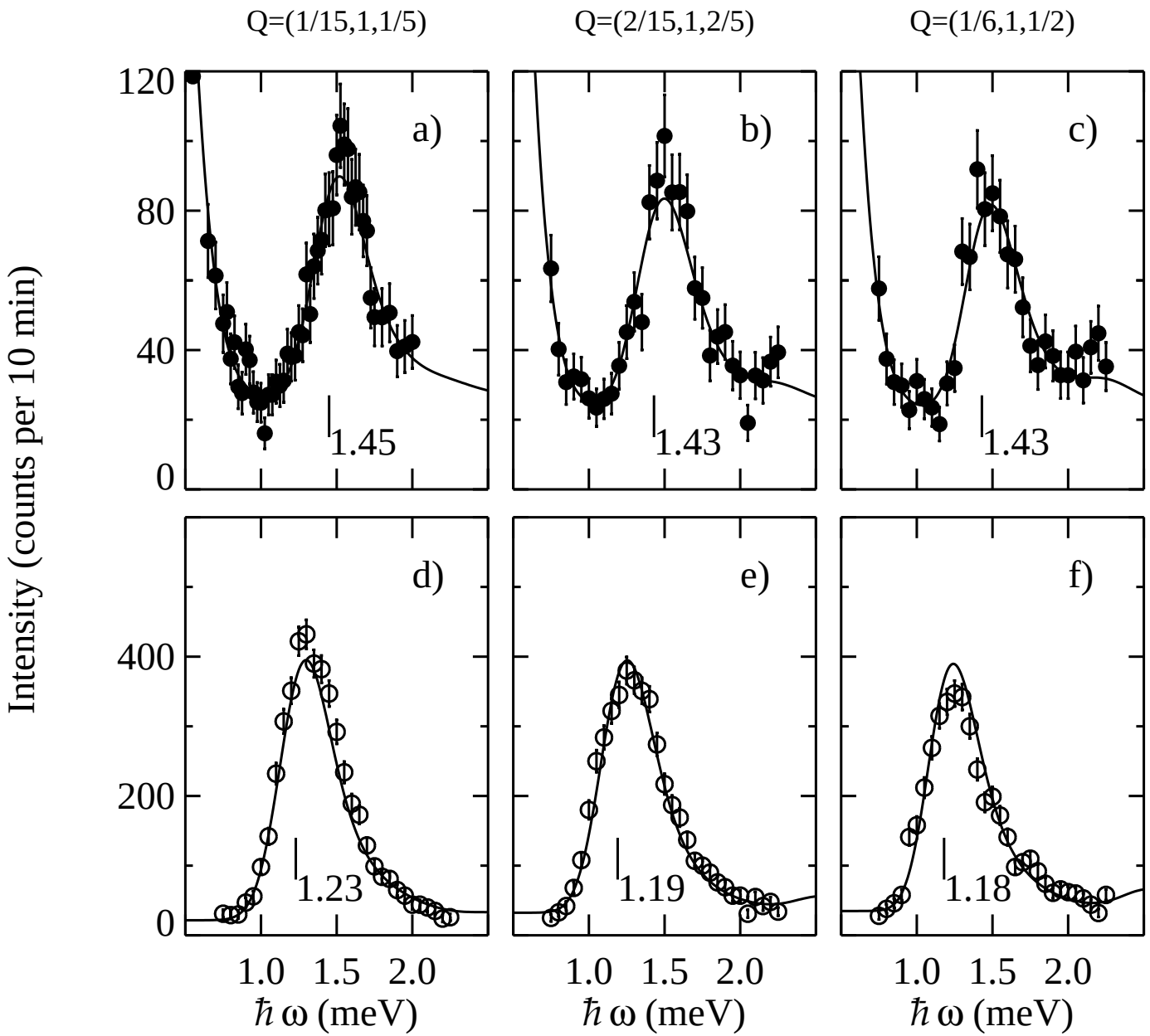
Q=(1/15,1,1/5)
Q=(2/15,1,2/5)
Q=(1/6,1,1/2)
Intensity (counts per 10 min)
120
80
40
0
400
200
0
a)
b)
c)
d)
e)
f)
1.45
1.43
1.43
1.23
1.19
1.18
1.0 1.5 2.0
1.0 1.5 2.0
1.0 1.5 2.0
ħ ω (meV)
ħ ω (meV)
ħ ω (meV)

Figure 3

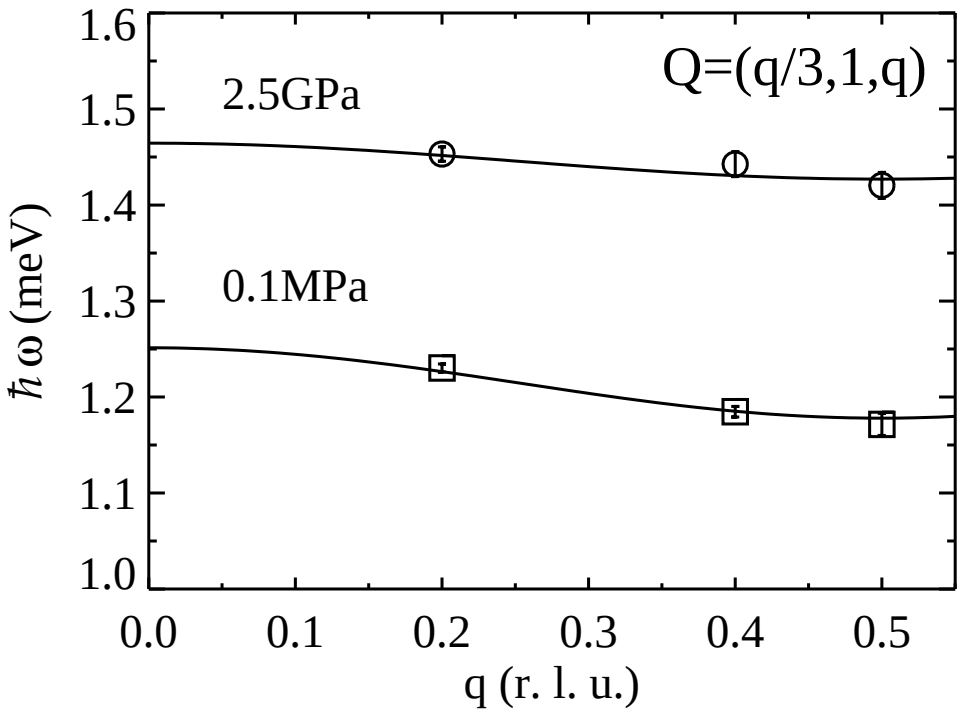
Q=(q/3,1,q)
2.5GPa
0.1MPa
ħω (meV)
q (r. l. u.)
1.6
1.5
1.4
1.3
1.2
1.1
1.0
0.0
0.1
0.2
0.3
0.4
0.5

Figure 4

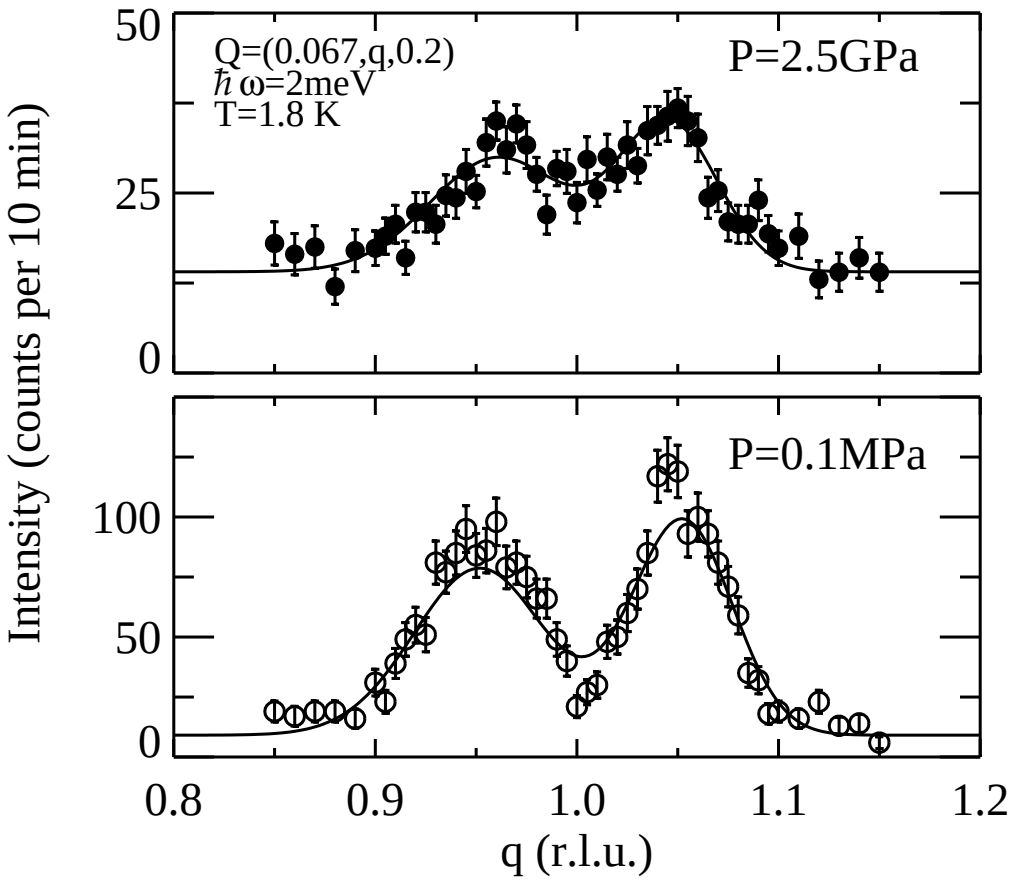
Q=(0.067,q,0.2)
ħω=2meV
T=1.8 K
P=2.5GPa
P=0.1MPa
Intensity (counts per 10 min)
q (r.l.u.)
50
25
0
100
50
0
0.8
0.9
1.0
1.1
1.2

Figure 5